Title
Electrochemical Lipolysis Induces Adipocyte Death and Fat Necrosis: In Vivo Pilot Study in Pigs

Journal
Plastic & Reconstructive Surgery, 153(2)

ISSN
0032-1052

Authors
Pham, Tiffany T
Heidari, Andrew E
Hong, Ellen M
et al.

Publication Date
2024-02-01

DOI
10.1097/prs.0000000000010645

Electrochemical Lipolysis Induces Adipocyte Death and Fat Necrosis: In Vivo Pilot Study in Pigs

Tiffany T. Pham, MD, MS[1,2]
Andrew E. Heidari, PhD[1,3]
Ellen M. Hong, BA[1]
Earl Steward, BS[4]
Yueqiao Qu, PhD[1,3]
Lily Y. Chen, BS[1]
Brandyn S. Dunn, MD[1,5]
Soo Hong Seo, MD[6]
Adeela Syed, PhD[7]
Katelyn Dilley, BS[1]
Lauren Lee, BS[1]
Dana M. Hutchison, MD, MS[1]
Kyle D. Hansen, BS[1]
Urja Patel, BS[1]
Sehwan Kim, PhD[8]
Michael G. Hill, PhD[9]
Brian J. F. Wong, MD, PhD[1,2,4]

Irvine, Orange, and Los Angeles, CA; Aurora, CO; and Seoul and Chungnam, Republic of Korea

Background: Current minimally invasive fat reduction modalities use equipment that can cost thousands of U.S. dollars. Electrochemical lipolysis (ECLL), using low-cost battery and electrodes (approximately $10), creates acid/base within fat (width, approximately 3 mm), damaging adipocytes. Longitudinal effects of ECLL have not been studied. In this pilot study, the authors hypothesize that in vivo ECLL induces fat necrosis, decreases adipocyte number/viability, and forms lipid droplets.

Methods: Two female Yorkshire pigs (50 to 60 kg) received ECLL. In pig 1, 10 sites received ECLL, and 10 sites were untreated. In pig 2, 12 sites received ECLL and 12 sites were untreated. For ECLL, two electrodes were inserted into dorsal subcutaneous fat and direct current was applied for 5 minutes. Adverse effects of excessive pain, bleeding, infection, and agitation were monitored. Histology, live-dead (calcein, Hoechst, ethidium homodimer-1), and morphology (Bodipy and Hoechst) assays were performed on day 0 and postprocedure days 1, 2, 7, 14 (pig 1 and pig 2), and 28 (pig 2). Average particle area, fluorescence signal areas, and adipocytes and lipid droplet numbers were compared.

Results: No adverse effects occurred. Live-dead assays showed adipocyte death on the anode on days 0 to 7 and the cathode on days 1 to 2 (not significant). Bodipy showed significant adipocyte loss at all sites ($P < 0.001$) and lipid droplet formation at the cathode site on day 2 ($P = 0.0046$). Histology revealed fat necrosis with significant increases in average particle area at the anode and cathode sites by day 14 (+277.3% change compared with untreated, $P < 0.0001$; +143.4%, $P < 0.0001$) and day 28 (+498.6%, $P < 0.0001$; +354.5%, $P < 0.0001$).

Conclusions: In vivo ECLL induces fat necrosis in pigs. Further studies are needed to evaluate volumetric fat reduction. *(Plast. Reconstr. Surg.* 153: 334e, 2024.)

Clinical Relevance Statement: In vivo ECLL induces adipocyte death and fat necrosis. ECLL has the potential to be utilized in body fat contouring.

Fat contouring has trended from invasive surgery to nonsurgical modalities, with 140,314 nonsurgical fat reduction procedures performed in 2020.[1–3] Existing minimally invasive treatments can entail high-cost equipment. Current radiofrequency,[4,5] high-intensity focused ultrasound,[6,7] cryolipolysis,[8,9] and laser lipolysis[10,11] medical devices range in cost from one to several tens of thousands of U.S. dollars. The cost of a laser source, which primarily makes up laser lipolysis devices,[12] can be upward of $1500.[13] In addition, deoxycholic acid,[14] as a nonregulated commercial product, can cost almost $500 for 100 mg of product.[15] To overcome such limitations, we have investigated a potential

From the [1]Beckman Laser Institute & Medical Clinic, [3]Department of Biomedical Engineering, and [7]Department of Developmental and Cell Biology, University of California, Irvine; [2]Department of Otolaryngology–Head and Neck Surgery, University of Colorado, School of Medicine; Departments of [4]Surgery and [5]Otolaryngology–Head and Neck Surgery, University of California, Irvine, School of Medicine; [6]Department of Dermatology, Korea University, College of Medicine; [8]Beckman Laser Institute-Korea, Dankook University; and [9]Department of Chemistry, Occidental College.
Received for publication March 14, 2021; accepted January 9, 2023.
Presented at the 12th International Symposium of Facial Plastic Surgery, in Dallas, Texas, October 15 through 18, 2018.

DOI: 10.1097/PRS.0000000000010645

Disclosure statements are at the end of this article, following the correspondence information.

Related digital media are available in the full-text version of the article on www.PRSJournal.com.

new, low-cost, nonsurgical fat reduction modality involving the use of in situ water hydrolysis to modify the biochemical and physical tissue properties. We have demonstrated that in situ water electrolysis to generate acid (at the anode) and base (at the cathode) can modify cartilage pliability,[16–32] cause localized collagen injury to skin,[33–37] and induce adipocyte necrosis and lipolysis when applied to fat.[38,39] In this latter application, referred to as electrochemical lipolysis (ECLL), saline is first injected into fat for tumescence and to increase tissue electrical conductivity. Subsequently, platinum electrodes are inserted through the fat. A potential is then applied from a direct current power supply, through which pH gradients (width, approximately 3 mm) are formed by means of water oxidation. In effect, ECLL induces acute adipocyte necrosis through membrane lysis, nuclear degradation, and lipolysis—the hydrolysis of triglycerides (TGs) into fatty acids and glycerol, as evidenced in our prior ex vivo studies using porcine tissue (Fig. 1).[39] In our prior experiments, approximately 40% of the TG mass liberated during cathodic ECLL was hydrolyzed into free fatty acids and glycerol, whereas anodic ECLL resulted in hydrolysis of approximately 48% of liberated TGs.[39] Electrochemical lipolysis is both simple and inexpensive, requiring a power supply and needle electrodes in its basic form, which could be manufactured for approximately $10.[35]

Our research group has developed mathematical models to guide ECLL dosimetry that estimate the electrical field specific to electrode geometry.[33–35,39] However, these numeric models do not easily evaluate how live biological tissues heal and respond to injury.[40] In this pilot study, we examine the in vivo longitudinal effects of ECLL in pigs, using histology and fluorescence microscopy assays for adipocyte viability and morphology. Given what is known about wound healing after chemical injury,[41,42] we hypothesize that ECLL decreases adipocyte viability and number, forms lipid droplets, and induces fat necrosis.

MATERIALS AND METHODS

Study Design

Two female Yorkshire pigs (50 to 60 kg) received ECLL on their dorsum with multiple treatment sites to determine the longitudinal effect of ECLL (Fig. 2). Two sites on the pig dorsum were allocated for untreated controls and two sites were allocated for ECLL treatment for each evaluation time point: day 0 (2 hours after the procedure) and days 1, 2, 7, and 14 for the

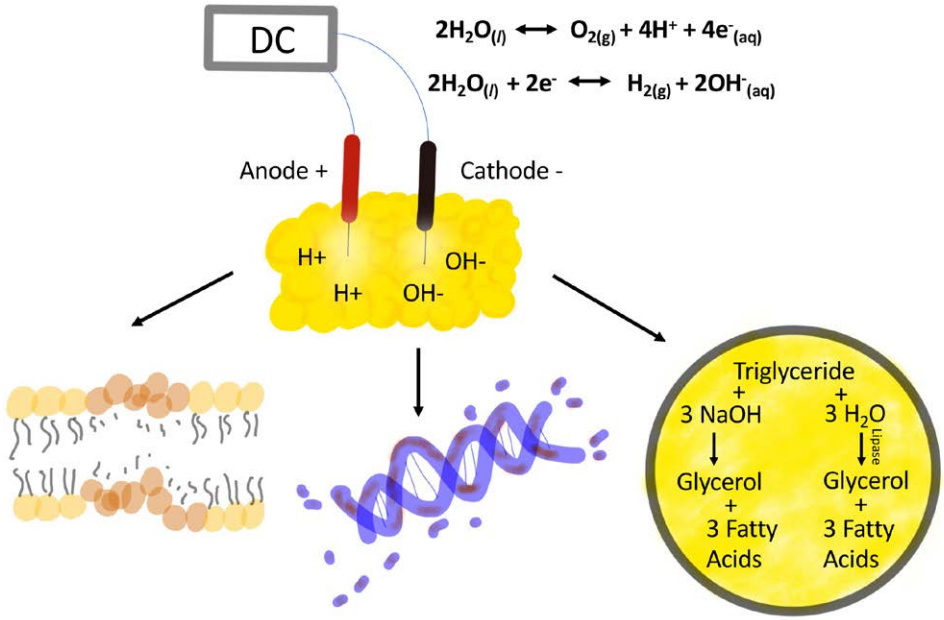

Fig. 1. Biomechanisms of ECLL. (*Above*) In ECLL, two platinum electrodes are inserted into fat tissues after saline injection. A direct current is then applied to the fat with current drawn from a power supply, creating in vivo H+ ions at the anode electrode and OH– ions at the cathode electrode. ECLL destroys adipocytes by means of (*below*, *left*) membrane lysis, (*below*, *center*) nuclear degradation, and (*below*, *right*) saponification of TGs.

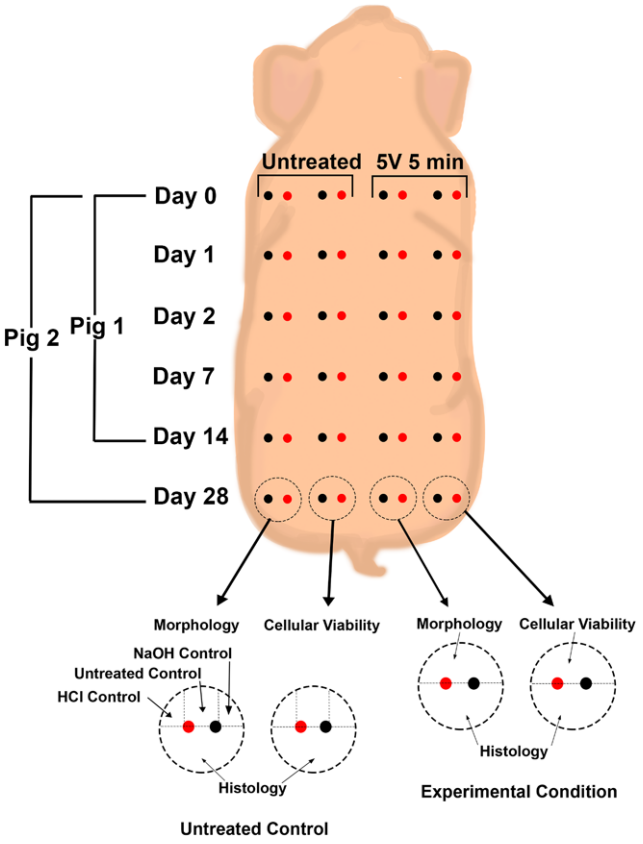

Fig. 2. Illustration of ECLL treatment grid applied to the dorsal surface of pigs. Each experimental area was treated with saline tumescence and ECLL at 5 V for 5 minutes. Anode (*red*) and cathode (*black*) sites are denoted by *colored pinpoint circles*. On the opposite side, matched control sites were placed where sham treatment (saline and electrode insertion only without ECLL treatment) was performed. Ten-millimeter punch biopsy specimens, shown by a *dotted circle*, were obtained on each experimental day for further analysis by histology, and morphologic and viability fluorescent microscopy assays.

first pig; and day 0 (2 hours after the procedure) and days 1, 2, 7, 14, and 28 for the second pig. For the first pig, a total of 10 sites were treated with ECLL and 10 sites were untreated, whereas for the second pig, there was a total of 12 ECLL treated sites with 12 untreated sites. Each site was 3.5 × 2.5 cm from the adjacent site. Tissue biopsy specimens (20 biopsy specimens for pig 1 and 24 biopsy specimens for pig 2) were acquired at each time point for histology and fluorescence assays to assess adipocyte viability and morphology. In investigating ECLL's ability to induce fat necrosis, the primary outcome of the study was to show at least a 30% statistically significant increase in average particle area of lipid droplets and adipocytes in histology in adipose tissue at sites treated with ECLL compared with the untreated sites at day 28. Secondary outcomes included at least a statistically significant 30% decrease in the number of adipocytes at day 28, and a statistically significant 30% increase in lipid droplets at day 0 at ECLL-treated sites compared with untreated sites. Furthermore, another secondary outcome of the study was to show 30% decreased calcein-AM (calcein) fluorescent signal area and 30% increased ethidium homodimer-1 (EthD-1) signal area to show decreased cell viability at ECLL-treated sites compared with untreated sites at day 0. Pigs were killed humanely with intravenous pentobarbital sodium/phenytoin sodium (0.3 mL/kg). The protocol was performed in accordance with the institutional animal care and use committee of the University of California, Irvine (AUP-17-164).

Animal Anesthesia

Pigs were injected intramuscularly with Telazol (10 to 11 mg/kg) and xylazine (4 to 5 mg/kg) for sedation. Enrofloxacin (7.5 mg/kg) was given intramuscularly for antibiotic prophylaxis. Pigs were intubated and ventilated. Isoflurane gas (1% to 3%) was administered continuously during procedures. Tidal volume (10 mL/kg initially, then adjusted to maintain 35 to 40 mmHg carbon dioxide), respiratory rate (12 breaths/min), and mechanical ventilation (inspiratory-to-expiratory ratio, 1:2) were maintained during anesthesia. Lactated ringer solution was administered intravenously or subcutaneously for hydration.

ECLL Procedure

Following shaving, normal saline (1 mL) was injected into subcutaneous fat at each treatment site. Following cannulation by means of a 25-gauge hypodermic needle, 30-gauge platinum needle electrodes (Natus, Pleasanton, CA) were inserted 3 mm apart and 1 cm deep into the skin and subcutaneous tissues. Using a direct current power supply, ECLL was administered at 5 V (transferred charge average 1.7 ± 0.18 coulomb) for 5 minutes while monitoring current. The untreated control followed an identical procedure as previously mentioned without current application. Six 2-mm tattoos indicating x and y planes of electrode sites were placed for colocalization. Ten-millimeter punch biopsy specimens of skin and subcutaneous tissue at control and treatment sites were attained and cross-sectioned; each half was used for the experiments below. Biopsy sites were sutured and covered with Telfa pads (Covidien, Minneapolis, MN); Tegaderm film (Covidien, Minneapolis, MN); Ioban drapes

(3M, St. Paul, MN); and lastly, Spandage mesh (Medi Tech, Westwood, MA). After procedures, pigs were monitored daily for excessive pain (limitations to movement or feeding), agitation (aggressive behavior), excessive bleeding (bleeding that persists after holding pressure), and infection (localized warmth, erythema, swelling, drainage).

Tissue Staining Using Fluorescent Dyes

Cross-sectioned biopsy specimens of untreated sites were sliced into thirds and submerged for 2 hours in 1 N hydrochloric acid (HCl) or 10 N sodium hydroxide (NaOH) (Thermo Fisher, Waltham, MA) for positive controls, or wrapped in Hank's Balanced Salt Solution–soaked gauze for untreated controls.

Morphology Assay

Untreated and HCl-, NaOH-, and ECLL-treated specimens were stained with 800 μL of Bodipy 558/568 C12 (10 μg/mL) and Hoechst 33342 (2.5 μg/mL) (Invitrogen, Carlsbad, CA) at 37°C for 45 minutes. Bodipy, a lipophilic dye, provided morphologic and structural tissue information of adipocytes and lipid droplets. Hoechst, a cell-permeable dye, was used to counterstain DNA of cells regardless of viability status, thus differentiating adipocytes (with nuclei emitting blue fluorescence) and lipid droplets (without nuclei).

Live-Dead Assay

Specimens were stained with 800 μL of calcein (10 μg/mL), EthD-1 (0.75 μg/mL) (Invitrogen E1169, Carlsbad, CA), and Hoechst 33342 (2.5 μg/mL) at 37°C for 45 minutes. Calcein is a nonfluorescent cell-permeable dye that is cleaved by intracellular cytoplasmic esterases of live cells to calcein. In cells with intact membranes, calcein—which emits a green fluorescence signal—is retained. Ethidium homodimer, a nonpermeable DNA stain, was used to stain nuclei of dead cells with damaged membranes, emitting red fluorescence. Hoechst was used to stain nuclei of all cells. With this combination, loss of cytoplasmic green calcein signal and nuclear blue Hoechst signal, and the increased nuclear red EthD-1 signal, indicates the loss of cell viability and cell death. Samples were washed before imaging.

Confocal Fluorescence Microscopy

An inverted confocal laser scanning microscope (ZEISS LSM780; Carl Zeiss, Jena, Germany) with a 10× objective lens was used to acquire Z-stacks (1416.99 × 1416.99 μm^2). Representative areas with high concentrations of adipocytes were selected for imaging. The lasers were centered at 405, 488, and 514 nm. Peak excitation/emission wavelengths of the dyes are as follows: Bodipy (543/568 nm), Hoechst 33342 (400/497 nm), calcein (488/515 nm), and EthD-1 (543/617 nm).

Quantification of Fluorescence Assays

For the morphology assay, adipocytes and lipid droplets were counted manually with Fiji (ImageJ) software by three trained counters blinded to treatment conditions. Adipocytes included well-formed Bodipy staining with eccentric nuclei Hoechst staining. Lipid droplets contained Bodipy staining without Hoechst staining.

To quantify the live-dead assay, a custom Fiji macromeasured the fluorescence signal area for each channel. Intensity thresholding was first performed for each channel to remove background noise. Second, the intensity threshold was converted into a binary mask. The areas of individual discrete elements of the binary mask were measured for each condition.

Histology with Quantitative Analysis

Tissues were fixed in 10% buffered formalin, processed, and paraffin embedded.[43] Eight-micron-thick slides were stained with hematoxylin and eosin. At least three slides per treatment condition were evaluated by two observers. Representative images of untreated and ECLL-treated sites were acquired using a light microscope (Olympus). Average particle area was calculated using Fiji.[44] Histologic images at 50× were thresholded by intensity to create a binary mask of lipids present (lipid droplets and adipocytes) and subsequently underwent binary watershed segmentation. The Fiji particle analysis algorithm calculated each particle area.

Statistical Analysis

Statistical analysis was performed using PRISM (v9.3.0; GraphPad, San Diego, CA). The Shapiro-Wilk test was used for normality testing. The morphology and histology data were found to be distributed normally. One-way analyses of variance with post hoc Tukey *t* tests were performed for the morphology data. Two-way analyses of variance with post hoc Tukey *t* tests were performed for histology. As the live-dead fluorescence data were not distributed normally, the Kruskal-Wallis nonparametric test was performed. Statistical significance was determined at values of $P \leq 0.05$,

$P \leq 0.01$, and $P \leq 0.001$. All parametric data are expressed as mean, SEM, and percentage change. Nonparametric live-dead fluorescence data are expressed as median and interquartile range.

RESULTS

All animals survived the study's duration. No adverse effects of excessive pain, excessive bleeding, infection, or animal agitation was noted.

ECLL Induces Tissue Inflammation and Fat Necrosis

Histology (10×) showed that ECLL induced tissue inflammation and necrosis (Fig. 3). The untreated control showed normal fat tissue architecture. On day 0 at the cathode, adipocytes without clear nuclei were shown. On day 7 at both electrode sites, anucleated adipocytes with mixed inflammatory and fibroblast infiltrate along the periphery of the injured area were shown. On day 28, fat necrosis at both electrode sites was shown.

Further microscopic histologic characteristics were visualized at 50× magnification (Fig. 4). Untreated control showed regular adipocyte spherical morphology and eccentric nuclei. At the cathode on days 0 to 7, adipocyte nuclei were lost. On days 1, 2, and 7 at the anode, nuclei were lost and adipocyte morphology was significantly altered. On day 7 at the anode and day 14 at both electrode sites, lymphocytes and macrophages (with some plasma cells and neutrophils) were present on the periphery of treated areas, in addition to fibroblasts and fibrosis surrounding lipid droplets. On day 14, inflammatory infiltrates traveled to the central treatment area. Foamy macrophages filled with lipids were present at both electrode sites. Fat necrosis (with macrocystic and microcystic fat changes with associated fibrosis) occurred on days 14 and 28.

Particle area of lipid droplets and adipocytes is denoted in Figure 4, *below* and summarized in Table 1. Compared with the untreated sites, days 2, 14, and 28 showed statistically significantly increased average particle area at the anode [9537.9 ± 619.1 μm^2 (mean ± SEM), +47.0%, $P = 0.0025$; 25,325.1 ± 5724.7 μm^2, +277.3%, $P < 0.0001$; and 38,420.2 ± 28,420.2 μm^2, +498.6%, $P < 0.0001$; respectively] and cathode [9255.3 ± 677.3 μm^2 (mean ± SEM), +42.6%, $P = 0.0066$; 16,338.8 ± 3671.7 μm^2, +143.4%, $P < 0.0001$; and 29,169.2 ± 13,525.8 μm^2, +354.5%, $P < 0.0001$, respectively]. There were no statistically significant differences in particle area at the untreated sites for all time points.

ECLL Induces Lipid Droplet Formation with Loss of Fat Staining

Adipocyte and lipid droplet morphology findings are shown in Figure 5. Untreated control Bodipy fluorescence showed circular adipocytes

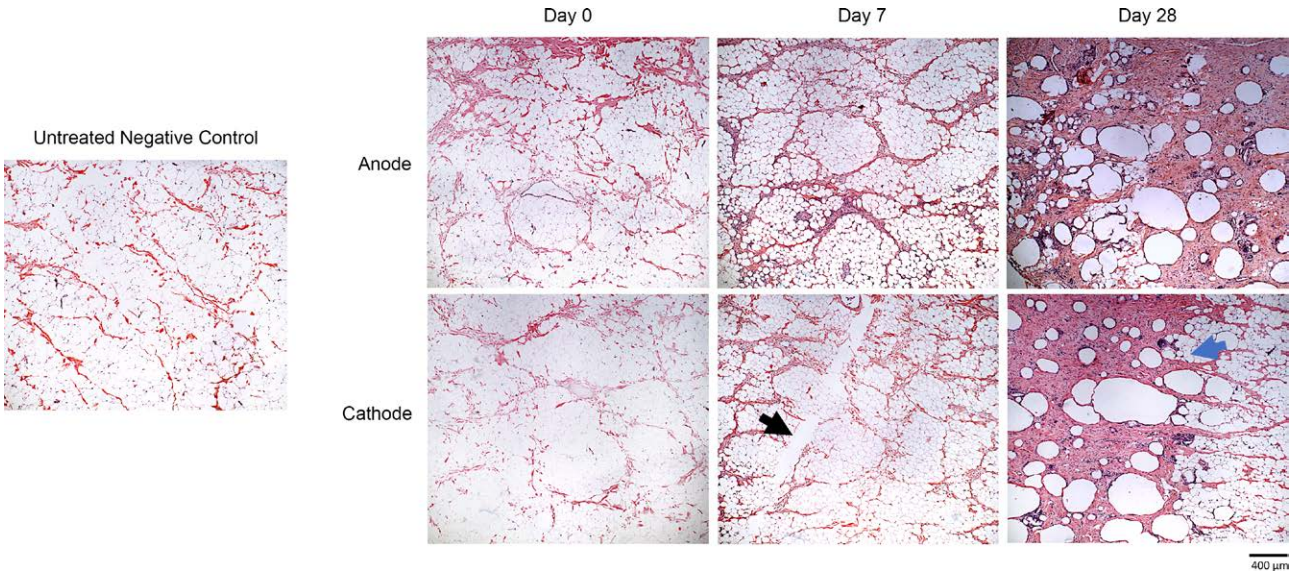

Fig. 3. Hematoxylin and eosin histology at 10× magnification of adipose tissue illustrating the longitudinal effects of ECLL. (*Left*) Untreated control, (*Right, above* panels) anode region, and (*Right, below* panels) cathode region. (*Below, second from right*) An electrode insertion site is depicted by an outline of the electrode. (*Below, right*) Spatial selectivity of ECLL-induced adipocyte necrosis at the cathode region adjacent to unaffected tissue. *Black arrow*, electrode insertion site; *Blue arrow*, demarcation between cathode and untreated areas. *Scale bars* = 400 µm.

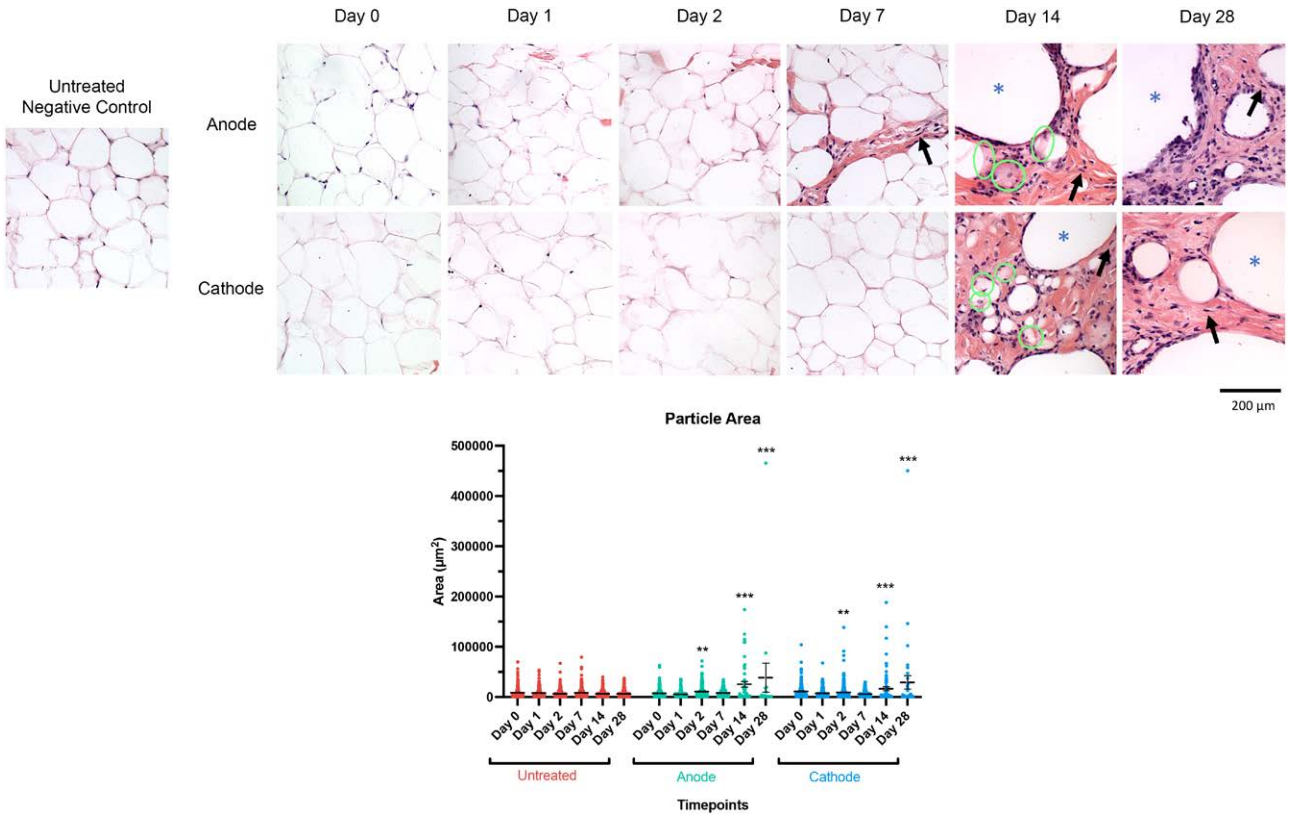

Fig. 4. Hematoxylin and eosin histology at 50× magnification of adipose tissue illustrating the longitudinal effects of ECLL. (*Left*) Untreated control, (*right, above* panels) longitudinal representation of adipose tissue surrounding the anode electrode of a 5-V, 5-minute ECLL treatment, and (*right, center* panels) longitudinal representation of adipose tissue surrounding the cathode electrode of a 5-V, 5-minute ECLL treatment. *Green circle*, foamy macrophages; *blue asterisk*, macrocyst; *black arrow*, fibroblast. *Scale bars* = 200 μm. (*Below*) Particle area of lipid droplets and adipocytes are shown at the untreated, anode, and cathode sites, with average and SEM bars. Statistical significance was determined at $*P \leq 0.05$, $**P \leq 0.01$, and $***P \leq 0.001$.

containing eccentric nuclei, organized into lobules, with minimal lipid droplet formation. Acutely, HCl-treated tissues showed statistically significantly fewer adipocytes (160 versus 363.3; $P = 0.001$). Damage was greater in NaOH-treated tissues with complete adipocyte destruction (0 versus 363; $P < 0.0001$) and decreased staining and no nuclear Hoechst signals. In ECLL specimens over 28 days, there was a substantial loss in Bodipy staining of lipids after ECLL at both anode and cathode electrodes, particularly on days 14 and 28. Compared with the untreated site, the mean numbers of adipocytes in all conditions and time points were statistically significantly decreased (Table 2). Compared with untreated, there was a statistically increased mean number of lipid droplets in anode on day 1 (504.0 versus 183.0; $P = 0.0260$) and cathode on day 2 (560.7 versus 183.0; $P = 0.0046$) (Table 3). Notably, nuclear Hoechst staining of adipocytes near the anode was present on day 0, and diminished through day 28. The cathodes revealed diminished nuclear Hoechst adipocyte staining on day 1 and continued to diminish through day 28. Hoechst stain surrounding remnant adipocytes and lipid droplets on days 7, 14, and 28 at the cathode sites and days 14 and 28 at the anode sites was visualized. Descriptive morphology assay findings are summarized. (**See Table, Supplemental Digital Content 1**, which shows a descriptive summary of morphology assay findings, ***http://links.lww.com/PRS/G415***.)

ECLL Degrades Adipocyte Nuclei and Induces Cell Death

Findings of the live-dead assay are shown in Figure 6. Comparisons are made between mean EthD-1 (Table 4), Hoechst (Table 5), and calcein signal areas of untreated and ECLL-treated sites; however, there were no statistically significant differences (Table 6). In the untreated control, intact live adipocytes were represented by cytoplasmic calcein signal with nuclear Hoechst signal. Conversely, HCL-treated tissues showed

Table 1. Comparisons of Average Particle Area of Lipid Droplets and Adipocytes in Histology

Comparisons	Average Particle Area (μm²)	SEM (μm²)	No.	Percentage Change (%)	*P*
Day 0					
Untreated vs.	8641.0	580.1	405		
Anode	6596.9	365.8	496	−23.7	0.0590
Cathode	8196.5	601.3	411	−5.1	0.8836
Day 1					
Untreated vs.	7912.5	609.8	219		
Anode	5589.0	291.8	602	−29.4	0.0716
Cathode	6737.3	338.0	517	−14.9	0.5216
Day 2					
Untreated vs.	6488.5	330.3	519		
Anode	9537.9	619.1	366	+47.0	0.0025[a]
Cathode	9255.3	677.3	375	+42.6	0.0066[a]
Day 7					
Untreated vs.	8222.3	694.5	213		
Anode	900.8	490.3	197	−3.9	0.9680
Cathode	5579.0	352.4	299	−32.1	0.0712
Day 14					
Untreated vs.	6712.7	306.6	482		
Anode	25,325.1	5724.7	49	+277.3	<0.0001[b]
Cathode	16,338.8	3671.7	77	+143.4	<0.0001[b]
Day 28					
Untreated vs.	6418.4	309.6	522		
Anode	38,420.2	28,420.2	16	+498.6	<0.0001[b]
Cathode	29,169.2	13,525.8	35	+354.5	<0.0001[b]

[a] *P* values of ≤ 0.01 were statistically significant.
[b] *P* values of ≤ 0.001 were statistically significant.

adipocyte membrane lysis and death with reduced mean calcein signal area (−96.8%) and increased mean EthD-1 signal area (+335.6%) compared with untreated tissue. NaOH-treated tissues demonstrated dead adipocytes with reduced mean calcein (−87.4%) and Hoechst (−66.4%) signal area.[45]

ECLL treatment at the anode on days 0 and 1 showed adipocyte death, with increased mean EthD-1 (+272.0% and +189.3%, respectively) and decreased mean calcein signal area (−99.4% and −98.3%, respectively). Days 2 and 7 involved decreased mean calcein signal area at the anode (−94.4% and −92.6%, respectively). On days 14 and 28, there was a decrease in mean calcein signal area (−33.7% and −41.2%, respectively) but pinpoint architecture, consistent with inflammatory and fibroblast infiltration seen in histology.

Similarly, at the cathode on day 0, the mean calcein signal area was decreased (−57.9%), with increased EthD-1 signal area (+471.5%), indicating membrane lysis and adipocyte cell death. Days 1 and 2 at the cathode showed little nucleic Hoechst staining (−20.6% and −10.7%, respectively), indicating nuclear degradation. Days 0 (−57.9%), 1 (−92.8%), 2 (−67.8%), 7 (−63.6%), 14 (−33.7%), and 28 (−41.2%) at the cathode showed diminished mean calcein signal area, suggesting continual adipocyte death. Days 2, 7, 14, and 28 showed pinpoint calcein signal and Hoechst signal illustrating inflammatory and fibroblast infiltrate most evident on days 14 and 28. The descriptive summary of the live-dead assay is shown. (**See Table, Supplemental Digital Content 2**, which shows a descriptive summary of live-dead assay findings, ***http://links.lww.com/PRS/G416***.)

DISCUSSION

Current minimally invasive modalities for fat contouring may require expensive equipment.[4,6,9,10,12,46] ECLL has been shown to damage adipocytes and saponify TGs,[38,39] a technique that can potentially be used for low-cost fat contouring. To move toward clinical evaluation, understanding how tissue injury following ECLL evolves over time is imperative. Using histology and fluorescence assays to investigate adipocyte viability and morphology, this pilot study demonstrates that in vivo ECLL lyses adipocytes and induces fat necrosis in pigs.

Controlled production of acid/base following ECLL[38,39] induces localized fat necrosis, as confirmed with histology. Acutely, ECLL induced

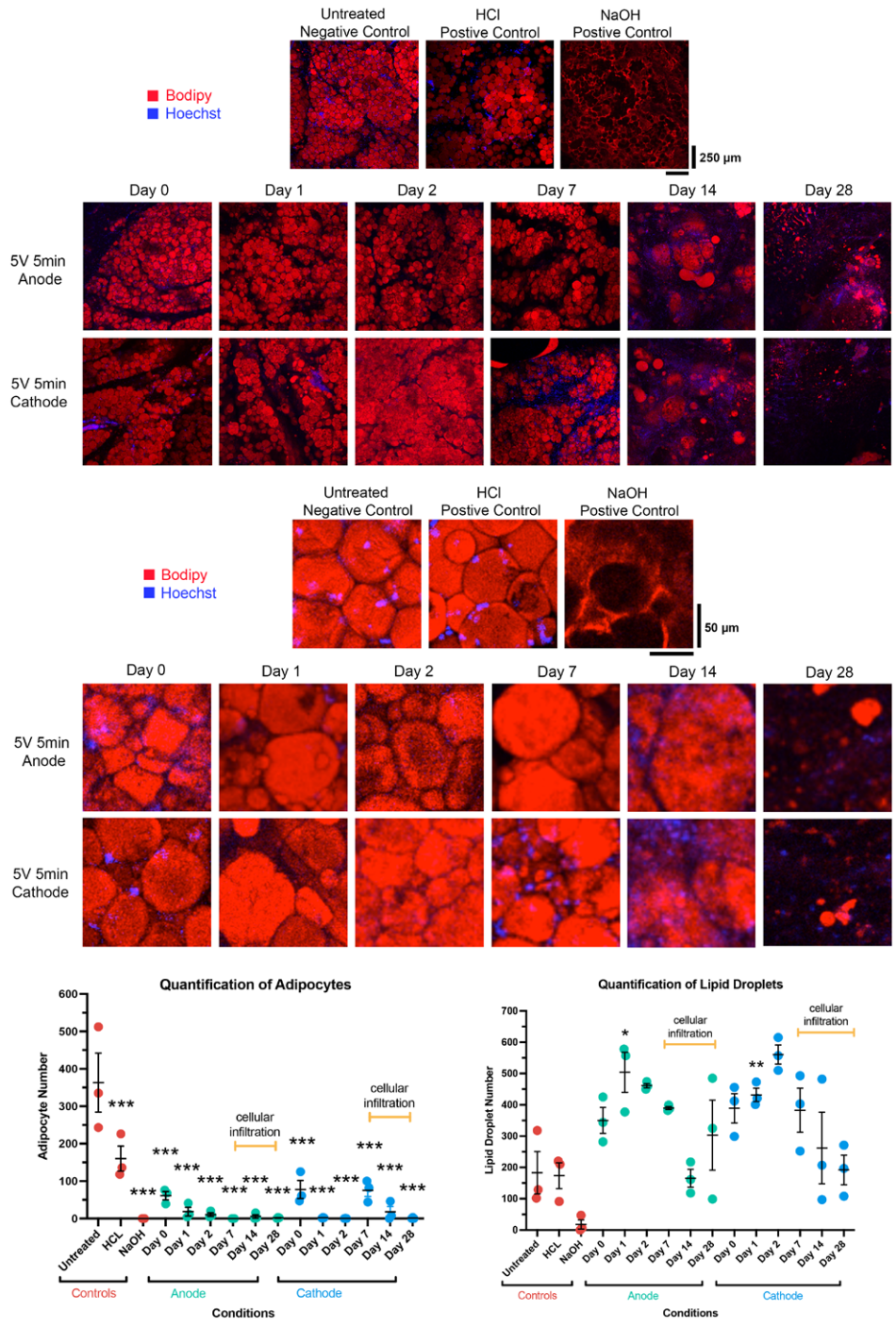

Fig. 5. Morphology assay with lipophilic Bodipy (*red*) and nuclear Hoechst (*blue*) stains. (*Above*) Representative fluorescence images of (*first row*) untreated control, HCl-treated tissue, and NaOH-treated tissue; (*second row*) longitudinal ECLL effect at the anode region; and (*third row*) longitudinal effects ECLL at the cathode region (*scale bars* = 250 μm). (*Center*) Higher magnification fluorescence images of (*fourth row*) untreated control, HCl-treated tissue, and NaOH-treated tissue; (*fifth row*) longitudinal ECLL effect at the anode region; and (*sixth row*) longitudinal effects ECLL at the cathode region (*scale bars* = 50 μm). (*Below*) Quantification of (*below, left*) adipocytes and (*below, right*) lipid droplets. Mean with SEM is shown. Statistical significance was determined at $*P \leq 0.05$, $**P \leq 0.01$, and $***P \leq 0.001$. *Yellow bars* indicate large infiltration of inflammatory cells and fibroblasts.

Table 2. Comparisons of Adipocyte Quantity in Morphology Assay

Comparisons	Mean Adipocyte No.	SEM	Percentage Change (%)	*P*[a]
Untreated vs.	363.3	78.9		
HCL	160.0	33.4	−56.0	0.0001
NaOH	0	0	−100	<0.0001
Anode				
Day 0	61.0	11.2	−83.2	<0.0001
Day 1	18.7	11.3	−94.9	<0.0001
Day 2	10.7	4.8	−97.0	<0.0001
Day 7	0	0	−100	<0.0001
Day 14	5.7	4.7	−98.4	<0.0001
Day 28	1.7	0.88	−99.5	<0.0001
Cathode				
Day 0	77.7	24.0	−78.6	<0.0001
Day 1	2.0	0.6	−99.4	<0.0001
Day 2	0.3	0.3	−99.9	<0.0001
Day 7	75.3	16.5	−79.3	<0.0001
Day 14	18.0	14.2	−95.0	<0.0001
Day 28	1.0	1.0	−99.7	<0.0001

[a] *P* values of ≤0.001 were statistically significant.

Table 3. Comparisons of Lipid Droplets Quantity in Morphology Assay

Comparisons	Mean Lipid Droplet No.	SEM	Percentage Change (%)	*P*
Untreated vs.	183.0	67.9		
HCL	173.7	41.4	−5.1	>0.9999
NaOH	17.7	14.8	−90.3	0.7646
Anode				
Day 0	350.3	41.4	+91.4	0.7504
Day 1	504.0	63.8	+175.4	0.0269[a]
Day 2	461.3	7.0	+152.1	0.0900
Day 7	389.7	5.0	+113.0	0.4435
Day 14	165.3	28.7	−9.7	>0.9999
Day 28	303.0	112.0	+65.6	0.9707
Cathode				
Day 0	389.0	46.8	+112.6	0.4485
Day 1	431.7	21.5	+135.9	0.1889
Day 2	560.7	30.4	+206.4	0.0046[b]
Day 7	382.7	70.3	+109.1	0.4974
Day 14	262.0	114.5	+43.2	0.9995
Day 28	192.0	47.1	+4.9	>0.9999

[a] *P* values of ≤ 0.05 were statistically significant.
[b] *P* values of ≤ 0.01 were statistically significant.

adipocyte membrane lysis, emptying of adipocytes with irregular membranes, and the formation of lipid droplets. In addition, adipocytes were enucleated at cathode and anode sites indicating nuclear degradation and fat necrosis.[47] Days 14 and 28 showed macrocystic and microcystic fat changes, occurring from irreversible adipocyte injury or acute inflammation.[48] Following ECLL, inflammatory cells were recruited, including predominantly lymphocytes and foamy macrophages (laden with lipid products released from dead adipocytes). These findings suggest the immediate effects of initiating cell death and the indirect response of inflammatory chemotaxis to the area. These inflammatory cells can also directly disrupt or indirectly destroy adipocyte membranes by means of cytokine or lytic enzyme release.[49] These histopathologic patterns are similar to phosphatidylcholine- and deoxycholate-induced effects of inflammation, fibrosis, and fat necrosis, as evaluated in various in vivo studies.[49–52]

Unlike histology which removes fat during processing, the use of Bodipy lipid staining with fresh tissue is effective in visualizing the presence of fat within adipocytes and lipid droplets. Bodipy staining illustrated adipocyte loss, lipid

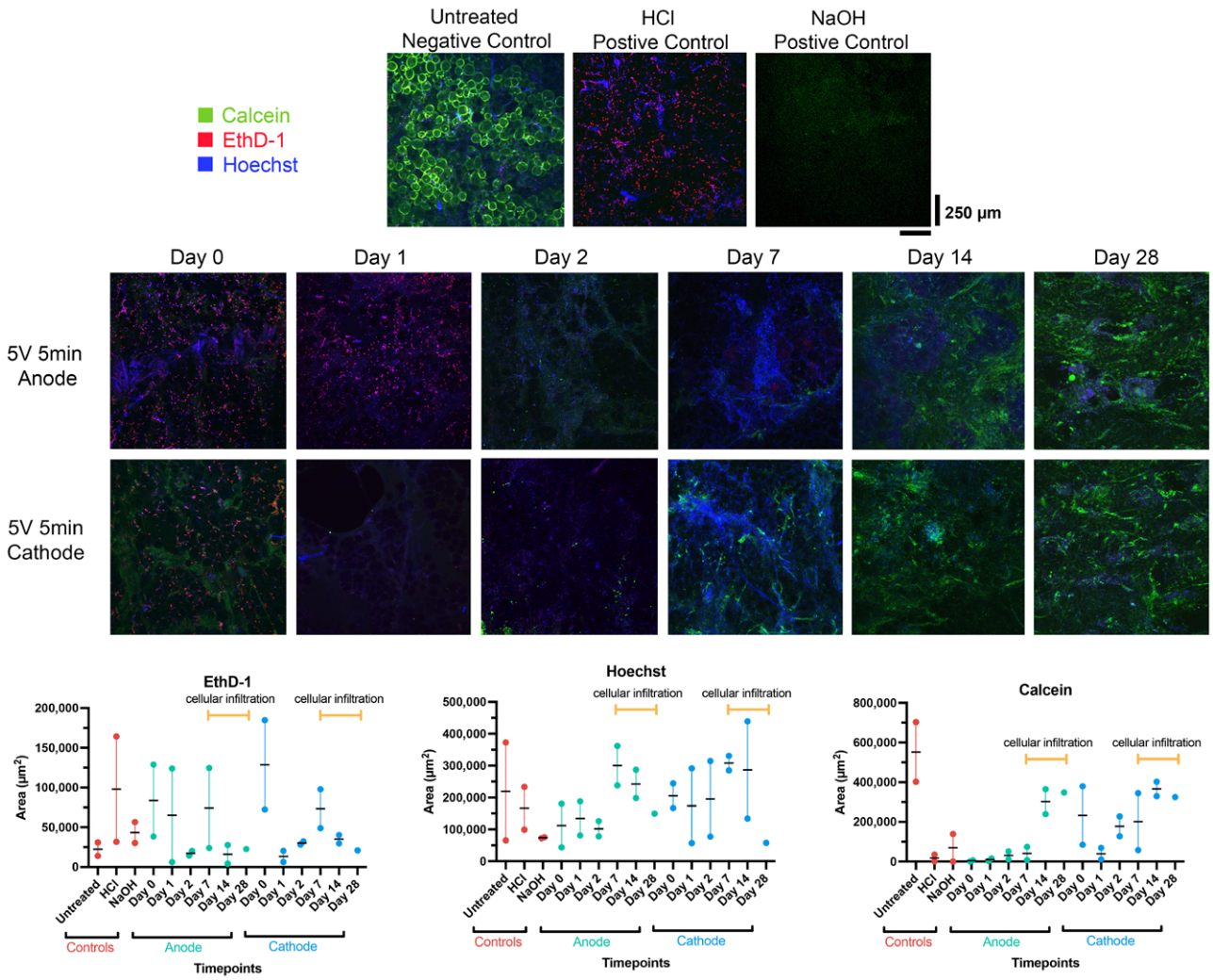

Fig. 6. Live-dead assay including cytoplasmic calcein (*green*), EthD-1 (*red*), and nuclear Hoechst (*blue*) stains. Representative fluorescence images of (*above*) untreated control, HCl-treated tissue, and NaOH-treated tissue; (*center*, *second row*) longitudinal ECLL effect at the anode region; and (*center, third row*) longitudinal effects ECLL at the cathode region (*scale bars* = 250 µm). (*Below*) Average fluorescence signal areas for controls and treated sites for (*below*, *left*) EthD-1, (*below*, *center*) Hoescht, and (*below*, *right*) calcein. Median with interquartile range is shown. *Yellow bars* indicate days with large infiltration of inflammatory cells and fibroblasts.

droplet formation, inflammation, and fat necrosis with ECLL. Loss of Bodipy staining was most significant on days 14 and 28, suggesting a loss of fat. However, adipocyte necrosis was clearly evident early at day 0, shown by diminished nuclear Hoechst staining. Similar findings of absent nuclear Hoechst staining have been observed to distinguish nonviable adipocytes from viable cells by Suga et al., who used various biochemical cell stains to evaluate liposuctioned fat samples.[53] The Hoechst staining around adipocytes most evident on days 14 and 28 again suggests inflammatory and fibroblast infiltration, with contribution of foamy macrophages in clearing the affected area of lipid products.

The lack of adipocyte calcein signal, with increased EthD-1 signal and diminished Hoechst signal, indicate adipocyte death, which is evident following ECLL. Combinations of these stains have been previously validated to assess adipocyte viability and death,[52,54] particularly with other minimally invasive adipose contouring techniques, including deoxycholate, phosphatidylcholine, and photobiomodulation.[49,55,56] ECLL also destroys adipocyte nuclei contributing to cell death, indicated by the loss of both nuclear EthD-1 and Hoechst signals, which begins earlier at the cathode site (day 1) than the anode site (day 2). Of note, histology showed clear enucleation earlier at the cathode site on day 0. The timing

Table 4. Comparisons of EthD-1 Signal Area in Live-Dead Assay

Comparisons	Median EthD-1 Signal Area (μm²)	IQR (μm²)	Percentage Change (%)	*P*
Untreated vs.	22,490.3	16,949.0		0.2310
HCL	97,962.0	132,482.1	+335.6	
NaOH	43,371.5	26,366.3	+92.8	
Anode				
Day 0	83,673.6	90,470.3	+272.0	
Day 1	65,055.2	117,577.7	+189.3	
Day 2	17,314.0	5,755.9	−23.0	
Day 7	74,223.9	100,561.5	+230.0	
Day 14	16,027.2	23,464.0	−28.7	
Day 28	22,591.3	Not applicable	+0.4	
Cathode				
Day 0	128,525.4	112,344.3	+471.5	
Day 1	13,485.6	13,988.6	−40.0	
Day 2	30,233.0	4,051.1	+34.4	
Day 7	73,458.2	48,929.3	+226.6	
Day 14	35,019.2	10,571.1	+55.7	
Day 28	20,852.6	Not applicable	−7.3	

Table 5. Comparisons of Hoechst Signal Area in Live-Dead Assay

Comparisons	Median Hoechst Signal Area (μm²)	IQR (μm²)	Percentage Change (%)	*P*
Untreated vs.	219,221.0	307,386.8		0.5648
HCL	166,382.9	134,526.6	−24.1	
NaOH	73,756.0	2,669.8	−66.4	
Anode				
Day 0	112,036.9	137,358.5	−48.9	
Day 1	134,415.2	107,050.4	−38.7	
Day 2	101,938.7	47,875.7	−53.5	
Day 7	300,083.2	123,674.6	+36.9	
Day 14	242,876.9	88,701.1	+10.8	
Day 28	149,202.2	Not applicable	−31.9	
Cathode				
Day 0	205,681.9	77,286.0	−6.2	
Day 1	174,160.3	234,410.7	−20.6	
Day 2	195,665.7	237,118.1	−10.7	
Day 7	307,951.6	45,692.2	+40.5	
Day 14	286,527.7	304,897.8	+30.7	
Day 28	57,663.4	Not applicable	−73.7	

difference may be related to increased sensitivity of biochemical dyes and functional imaging compared with hematoxylin and eosin visualization under light microscopy.

Through this study, we have investigated the longitudinal effects of ECLL treatment on subcutaneous porcine fat. Shown by means of histologic and biochemical fluorescence analysis, ECLL leads to adipocyte lysis, lipid droplet formation, and nuclear degradation; followed by inflammation, fibrosis, and fat necrosis and resorption. This method forms acid and base in situ, which can potentially be targeted to specific tissue locations for adipocyte death and subsequent body fat contouring. Insulating electrodes may easily obviate the skin effect. It is important to consider that ECLL's use may be limited in the patient population with implanted electrical devices, such pacemakers or cardioverter defibrillators.

Because of the costly and labor-intensive nature of survival studies, this pilot study has a small sample size of two animals; thus, power analysis was not performed and statistical comparisons were limited. At this current dosimetry, ECLL was shown to be safe and effective in inducing fat necrosis up to 28 days. At day 28, lipid deposits remain in the tissues and prevent the clinical observation of fat loss, which could potentially be observed after 3 months, as seen in other adipose contouring studies.[46,57] Thus, further studies with

Table 6. Comparisons of Calcein Signal Area in Live-Dead Assay

Comparisons	Median Calcein Signal Area (μm²)	IQR (μm²)	Percentage Change (%)	*P*
Untreated vs.	552,534.3	300,766.5		0.0866
HCL	17,788.5	34,019.7	−96.8	
NaOH	69,780.6	138,251.1	−87.4	
Anode				
Day 0	3559.6	5,327.1	−99.4	
Day 1	9494.6	11,885.2	−98.3	
Day 2	31,162.3	40,013.0	−94.4	
Day 7	41,139.4	66,507.9	−92.6	
Day 14	302,038.3	125,981.8	−45.3	
Day 28	348,486.9	Not applicable	−36.9	
Cathode				
Day 0	232,397.8	294,690.1	−57.9	
Day 1	39,899.5	58,429.2	−92.8	
Day 2	177,711.9	99,953.9	−67.8	
Day 7	201,374.7	287,224.0	−63.6	
Day 14	366,140.0	72,331.3	−33.7	
Day 28	324,967.0	Not applicable	−41.2	

larger sample sizes and longer survival times will assess macroscopic effects and evaluate the reabsorption of the saponified TGs induced by ECLL. Longer term studies will also elucidate any oil cyst formation (not seen in this current study), long-term fibrosis, skin dimpling, or skin laxity as potential complications. Future studies are also needed to investigate the effects of variations in geometric and temporal electrode distributions, which may alter the amount of adipose change or spatial effect and accuracy. If multiple needles or treatments are required for clinical fat volume changes, this technology may be limited by patient discomfort and inflammation. Although no excessive pain of the animal was observed in our study, future investigations of procedure-related pain without sedation are needed.

CONCLUSIONS

In this pilot study, we have demonstrated, by means of histology and fluorescence assays to assess adipocyte viability and morphology, that in vivo ECLL induces adipocyte death and fat necrosis in pigs. Further larger and longitudinal studies are needed to further confirm these findings. ECLL may eventually be adapted for procedures that alter adipose tissue morphology, such as in body fat contouring.

Brian J. F. Wong, MD, PhD
Beckman Laser Institute
1002 Health Sciences Road
Irvine, CA 92697
bjwong@uci.edu
Instagram: @brianwongmd

DISCLOSURE

The authors have no financial disclosures to report.

DISCLAIMER

The content of this article is solely the responsibility of the authors and does not necessarily represent the official views of the National Institutes of Health.

ACKNOWLEDGMENTS

This research was supported by the Irvine Head and Neck Research Foundation, Beckman Laser Institute Foundation, George E. Hewitt Foundation for Medical Research, University of California, Irvine, Applied Innovation POP award (443803-19954), a LAMMP grant funded by the National Institutes of Health/National Institute of Biomedical Imaging and Bioengineering (P41-EB015890), a Chao Cancer Center grant funded by the National Institutes of Health/National Cancer Institute (2P30CA062203-19), and the Leading Foreign Research Institute Recruitment Program through the National Research Foundation of Korea, funded by the Ministry of Science and ICT (2018K1A4A3A02060572). The authors thank Tatiana Krasieva, PhD, for assistance with fluorescence imaging; Naya Sterritt, Pranav Sreejith Nair, and Alexis Ha for assistance counting the morphology assay; and Lily Tran for assistance with preanimal study preparation.

REFERENCES

1. The Aesthetic Society. Aesthetic plastic surgery national databank statistics 2019. Available at: https://cdn.theaestheticsociety.org/media/statistics/2019-TheAestheticSocietyStatistics.pdf. Accessed April 9, 2022.

2. American Society of Plastics Surgeons. 2020 Plastic surgery statistics report. Available at: https://www.plasticsurgery.org/documents/News/Statistics/2020/plastic-surgery-statistics-full-report-2020.pdf. Accessed April 9, 2022.
3. Aesthetic plastic surgery national databank statistics 2020. *Aesthetic Surg J.* 2021;41(Suppl 2):1–16.
4. Blugerman G, Schavelzon D, Paul MD. A safety and feasibility study of a novel radiofrequency-assisted liposuction technique. *Plast Reconstr Surg.* 2010;125:998–1006.
5. Bimedis. Radio frequency units (RF) for sale. Available at: https://bimedis.com/search/search-items/cosmetic-equipment-radio-frequency-units-rf#:~:text=on the cheeks.-,How Much Does radio frequency machine cost%3F,much as 68 000 USD. Accessed September 3, 2022.
6. Saedi N, Kaminer M. New waves for fat reduction: high-intensity focused ultrasound. *Semin Cutan Med Surg.* 2013;32:26–30.
7. Pretty Lasers. HIFU machines for sale. Available at: https://www.prettylasers.com/hifu-machine-price/. Accessed September 3, 2022.
8. Bimedis. Zeltiq Coolscupting. Available at: https://bimedis.com/zeltiq-coolsculpting-m30501. Accessed September 3, 2022.
9. Ingargiola MJ, Motakef S, Chung MT, Vasconez HC, Sasaki GH. Cryolipolysis for fat reduction and body contouring: safety and efficacy of current treatment paradigms. *Plast Reconstr Surg.* 2015;135:1581–1590.
10. Avci P, Nyame TT, Gupta GK, Sadasivam M, Hamblin MR. Low-level laser therapy for fat layer reduction: a comprehensive review. *Lasers Surg Med.* 2013;45:349–357.
11. IBeautyMachine.com. Gentlipo Z; professional lipolaser slimming machine; i-lipo laser; fat removal; real Japan laser; high power; 208pcs laser lamp. Available at: https://www.ibeautymachine.com/professional/gentlipo-z-ilipo-lipolaser-body-slimming-machine.html. Accessed September 5, 2022.
12. Reynaud JP, Skibinski M, Wassmer B, Rochon P, Mordon S. Lipolysis using a 980-nm diode laser: a retrospective analysis of 534 procedures. *Aesthetic Plast Surg.* 2009;33:28–36.
13. Laser Diode Source. 980nm laser diode; up to 15 watts output power; SMA905 connector detachable fiber output. Available at: https://www.laserdiodesource.com/shop/980nm-15W-Fiber-Coupled-Module-RealLight. Accessed September 5, 2022.
14. Teller CF, Chiu A, Chesnut CD, et al. Best clinical practices with ATX-101 for submental fat reduction: patient-related factors and physician considerations. *Plast Reconstr Surg Glob Open* 2021;9:e3668.
15. Millipore Sigma. Deoxycholic acid. Available at: https://www.sigmaaldrich.com/US/en/search/deoxycholic-acid?focus=products&page=1&perpage=30&sort=relevance&term=%20deoxycholic%20acid&type=product_name. Accessed September 5, 2022.
16. Badran KW, Manuel CT, Loy AC, et al. Long-term in vivo electromechanical reshaping for auricular reconstruction in the New Zealand white rabbit model. *Laryngoscope* 2015;125:2058–2066.
17. Badran K, Manuel C, Waki C, Protsenko D, Wong BJF. Ex vivo electromechanical reshaping of costal cartilage in the New Zealand white rabbit model. *Laryngoscope* 2013;123:1143–1148.
18. Protsenko DE, Ho K, Wong BJF. Stress relaxation in porcine septal cartilage during electromechanical reshaping: mechanical and electrical responses. *Ann Biomed Eng.* 2006;34:455–464.
19. Manuel CT, Foulad A, Protsenko DE, Sepehr A, Wong BJF. Needle electrode-based electromechanical reshaping of cartilage. *Ann Biomed Eng.* 2010;38:3389–3397.
20. Protsenko DE, Lim A, Wu EC, Manuel C, Wong BJF. The influence of electric charge transferred during electromechanical reshaping on mechanical behavior of cartilage. In: *Proc. SPIE 7901, Energy-Based Treatment of Tissue and Assessment VI* 2011;790105:1–7.
21. Protsenko DE, Ho K, Wong BJF. Survival of chondrocytes in rabbit septal cartilage after electromechanical reshaping. *Ann Biomed Eng.* 2011;39:66–74.
22. Manuel CT, Foulad A, Protsenko DE, Hamamoto A, Wong BJF. Electromechanical reshaping of costal cartilage grafts: a new surgical treatment modality. *Laryngoscope* 2011;121:1839–1842.
23. Kuan EC, Hamamoto AA, Manuel CT, Protsenko DE, Wong BJF. In-depth analysis of pH-dependent mechanisms of electromechanical reshaping of rabbit nasal septal cartilage. *Laryngoscope* 2014;124:E405–E410.
24. Lim A, Protsenko DE, Wong BJF. Changes in the tangent modulus of rabbit septal and auricular cartilage following electromechanical reshaping. *J Biomech Eng.* 2011;133:094502.
25. Oliaei S, Manuel C, Karam B, et al. In vivo electromechanical reshaping of ear cartilage in a rabbit model: a minimally invasive approach for otoplasty. *JAMA Facial Plast Surg.* 2013;15:34–38.
26. Ho KHK, Valdes SHD, Protsenko DE, Aguilar G, Wong BJF. Electromechanical reshaping of septal cartilage. *Laryngoscope* 2003;113:1916–1921.
27. Hussain S, Manuel CT, Protsenko DE, Wong BJF. Electromechanical reshaping of ex vivo porcine trachea. *Laryngoscope* 2015;125:1628–1632.
28. Tracy LE, Wong BJ. The effect of pH on rabbit septal cartilage shape change: exploring the mechanism of electromechanical tissue reshaping. *Eplasty* 2014;14:e23.
29. Kim S, Manuel CT, Wong BJF, Chung P-S, Mo J-H. Handheld-level electromechanical cartilage reshaping device. *Facial Plast Surg.* 2015;31:295–300.
30. Manuel CT, Tjoa T, Nguyen T, Su E, Wong BJF. Optimal electromechanical reshaping of the auricular ear and long-term outcomes in an in vivo rabbit model. *JAMA Facial Plast Surg.* 2016;18:277–284.
31. Hunter BM, Kallick J, Kissel J, et al. Controlled-potential electromechanical reshaping of cartilage. *Angew Chemie Int Ed.* 2016;55:5497–5500.
32. Yau AYY, Manuel C, Hussain SF, Protsenko DE, Wong BJF. In vivo needle-based electromechanical reshaping of pinnae new Zealand white rabbit model. *JAMA Facial Plast Surg.* 2014;16:245–252.
33. Hu AC, Hong EM, Toubat O, et al. Multiphoton microscopy of collagen structure in ex vivo human skin following electrochemical therapy. *Lasers Surg Med.* 2020;52:196–206.
34. Pham TT, Hong EM, Moy WJ, et al. The biophysical effects of localized electrochemical therapy on porcine skin. *J Dermatol Sci.* 2020;97:179–186.
35. Moy WJ, Su E, Chen JJ, et al. Association of electrochemical therapy with optical, mechanical, and acoustic impedance properties of porcine skin. *JAMA Facial Plast Surg.* 2017;19:502–509.
36. Karlsmark T, Aalund O, Danielsen L, et al. The occurrence of calcium salt deposition on dermal collagen fibres following electrical injury to porcine skin. *Forensic Sci Int.* 1988;39:245–255.
37. Hutchison DM, Hakimi AA, Wijayaweera A, et al. Electrochemical treatment of ex vivo human abdominal skin and potential use in scar management: a pilot study. *Scars Burn Heal.* 2021;7:2059513120988532.

38. Hutchison DM, Hakimi AA, Hong EM, et al. Electrochemolipolysis of human adipose tissue. *Facial Plast Surg Aesthet Med*. 2020;22:86–92.
39. Pham TT, Stokolosa AM, Borden PA, et al. Electrochemical degradation and saponification of porcine adipose tissue. *Sci Rep*. 2020;10:1–15.
40. Boekema B, Ulrich MMW, Middelkoop E. Models for cutaneous wound healing. *Wound Repair Regen*. 2017;25:347–348.
41. Jeschke MG, van Baar ME, Choudhry MA, Chung KK, Gibran NS, Logsetty S. Burn injury. *Nat Rev Dis Prim*. 2020;6:11.
42. Palao R, Monge I, Ruiz M, Barret JP. Chemical burns: pathophysiology and treatment. *Burns* 2010;36:295–304.
43. Rolls G. Difficult blocks and reprocessing: what to do when your block won't section. *PathologyNews.com*. Melbourne: Leica Biosystems; 2016:1–107.
44. Osman OS, Selway JL, Kępczyńska MA, et al. A novel automated image analysis system for accurate adipocyte quantification. *Adipocyte* 2013;2:160–164.
45. Raap AK, Marijnen JGJ, Vrolijk J, van der Ploeg M. Denaturation, renaturation, and loss of DNA during in situ hybridization procedures. *Cytometry* 1986;7:235–242.
46. Wollina U, Goldman A. ATX-101 for reduction of submental fat. *Expert Opin Pharmacother*. 2015;16:755–762.
47. Segura S, Requena L. Anatomy and histology of normal subcutaneous fat, necrosis of adipocytes, and classification of the panniculitides. *Dermatol Clin*. 2008;26:419–424.
48. Adigun R, Bhimji SS. *Necrosis, Cell (Liquefactive, Coagulative, Caseous, Fat, Fibrinoid, and Gangrenous)*. Treasure Island, FL: StatPearls; 2018.
49. Rose PT, Morgan M. Histological changes associated with mesotherapy for fat dissolution. *J Cosmet Laser Ther*. 2005;7:17–19.
50. Schuller-Petrovic S, Wölkart G, Höfler G, Neuhold N, Freisinger F, Brunner F. Tissue-toxic effects of phosphatidylcholine/deoxycholate after subcutaneous injection for fat dissolution in rats and a human volunteer. *Dermatol Surg*. 2008;34:529–542; discussion 542–543.
51. Rittes PG, Rittes JC, Amary MFC. Injection of phosphatidylcholine in fat tissue: experimental study of local action in rabbits. *Aesthetic Plast Surg*. 2006;30:474–478.
52. Bechara FG, Mannherz HG, Jacob M, et al. Induction of fat cell necrosis in human fat tissue after treatment with phosphatidylcholine and deoxycholate. *J Eur Acad Dermatol Venereol*. 2012;26:180–185.
53. Suga H, Matsumoto D, Inoue K, et al. Numerical measurement of viable and nonviable adipocytes and other cellular components in aspirated fat tissue. *Plast Reconstr Surg*. 2008;122:103–114.
54. Conti G, Jurga M, Benati D, et al. Cryopreserved subcutaneous adipose tissue for fat graft. *Aesthetic Plast Surg*. 2015;39:800–817.
55. Caruso-Davis MK, Guillot TS, Podichetty VK, et al. Efficacy of low-level laser therapy for body contouring and spot fat reduction. *Obes Surg*. 2011;21:722–729.
56. Klein SM, Schreml S, Nerlich M, Prantl L. In vitro studies investigating the effect of subcutaneous phosphatidylcholine injections in the 3T3-L1 adipocyte model: lipolysis or lipid dissolution? *Plast Reconstr Surg*. 2009;124:419–427.
57. Avram MM, Harry RS. Cryolipolysis for subcutaneous fat layer reduction. *Lasers Surg Med*. 2009;41:703–708.